

Two-Dimensional Structures Formed by Triblock Patchy Particles with Two Different Patches

メタデータ	言語: eng 出版者: 公開日: 2022-12-15 キーワード (Ja): キーワード (En): 作成者: メールアドレス: 所属:
URL	https://doi.org/10.24517/00068485

This work is licensed under a Creative Commons Attribution-NonCommercial-ShareAlike 3.0 International License.



Two-Dimensional Structures Formed by Triblock Patchy Particles with Two Different Patches

Masahide Sato*

Emerging Media Initiative, Kanazawa University, Kanazawa 920-1192, Japan

E-mail: msato002@staff.kanazawa-u.ac.jp

Abstract

Two-dimensional structures formed by spherical triblock patchy particles are examined by performing Monte Carlo simulations. In the model, the triblock patchy particles have two different types of patches at the polar positions. The patch sizes are different from each other and the attractive interaction acts only between the same type of patches. The particles translate on a flat plane and rotate three-dimensionally. When varying the two patch sizes, the pressure, and interaction energy, various structures are observed. When the difference between two patch sizes is small, kagome lattices, hexagonal structures, two-dimensional dodecagonal quasi-crystal structures are observed. When the difference between two patch sizes is large, chain-like structures are created. With lower temperature, sparse structures such as ring-like structures form.

Introduction

Particles with patches whose properties are different from those of the other surface areas are known as patchy particles, and these make promising building blocks for functional materials such as photonic crystals.¹⁻⁶ Because the anisotropy and strength of attractive interactions can be controlled experimentally for patchy particles, by changing the patch materials and their number and locations, unique and complicated structures are expected to be more easily created with patchy particles than with isotropic particles.

The structures created by patchy particles with a single patch have been well studied,⁷⁻²⁰ showing that close packed structures with complicated bonding and various open structures can be created by controlling the patch area, the interaction length, and the interaction strength.

When considering triblock patchy particles, which have two patches on their surfaces, more complicated structures than those created by single-patch particles are possible in both three-dimensional²¹⁻²⁶ and two-dimensional systems.²⁷⁻³¹ As an example of an open structure, a kagome lattice can be created in a two-dimensional system.²⁷ When the two patch sizes are different from each other,²⁷⁻³¹ a ring-like structure²⁹ and some chain-like structures,³⁰ are observed owing to the formation of a Y-shaped bonding geometry, which is not observed in triblock patchy particles with uniformly sized patches. In three-dimensional systems²³⁻²⁶, open crystals are attractive materials, especially for use as photonic crystals,¹⁻⁶ and these are created effectively in particles with two patches with different sizes where the attractive interaction between the patches depends on the combination of patches. In the two-dimensional systems of triblock patchy particles, not only can structures be observed in experiments^{27,29,30} but also other structures which have yet to be experimentally observed may also be created when the two patch areas are different and the attractive interaction strength is dependent on the patch types.

Under the assumption that the two patch sizes are different and the attractive interaction acts only between the same type of patches, isothermal-isobaric Monte Carlo simulations with

Kern-Frenkel potential^{32,33} were performed to examine how many types of two-dimensional structures can be created when changing the two patch sizes, also examining their dependence on the pressure P and the interaction energy ϵ .

In this report, I introduce a model to simulate triblock patchy particles and their formed structures. Results are shown for typical snapshots, indicating dependence of structures on patch areas and noting effects of neglecting attractive interactions between different patches.

Method

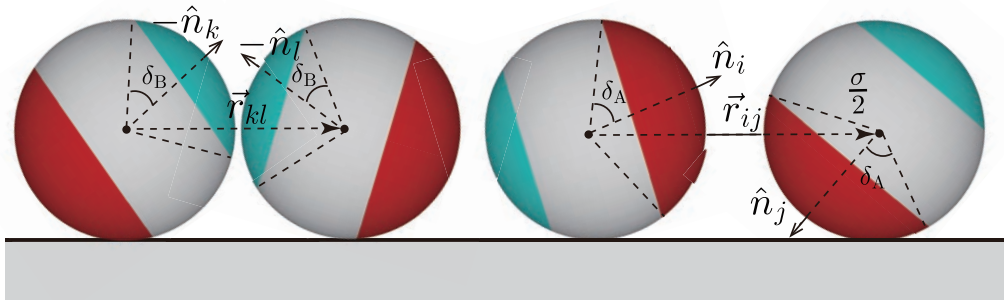


Figure 1: Schematic figure of the system used in simulations, with spherical patchy particles on a flat plane. The diameter of the particles is given by σ . Red and blue regions, which are in opposing directions, represent patch A and patch B, respectively. \hat{n}_i represents the direction of patch A for the i th particle, \vec{r}_{ij} represents the vector from the center of the i th particle to the j th particle, σ is the diameter of particle, and δ_A and δ_B are the angles indicating the sizes of patches A and B, respectively. The attractive interaction between patches acts only between patches of the same type.

Model Figure 1 shows the system I use in my simulations; spherical triblock patchy particles translated on a flat xy -plane rotating three-dimensionally. The patchy particles have two different types of patches, patch A and patch B, at the polar positions, with attractive interactions acting only between the same type of patch. The interaction potential between the patches is given by the Kern-Frenkel potential^{32,33}. The potential between the i th and

j th particles, $U^{\text{KF}}(r_{ij})$, is expressed as

$$U^{\text{KF}}(r_{ij}) = U_{\text{rep}}(r_{ij}) + U_{\text{SW}}(r_{ij})f(\hat{\mathbf{r}}_{ij}, \hat{\mathbf{n}}_i, \hat{\mathbf{n}}_j), \quad (1)$$

where \mathbf{n}_i represents the unit normal vector at the center of patch A of the i th particle, \mathbf{r}_i represents the position of the center of the i th particle, and $r_{ij} = |\mathbf{r}_{ij}| = |\mathbf{r}_i - \mathbf{r}_j|$. Because patch B is located opposite to patch A, the unit normal vector at the center of patch B is represented by $-\mathbf{n}_i$. $U_{\text{rep}}(r_{ij})$ is the hard-core repulsive interaction potential, which is given by

$$U_{\text{rep}}(r_{ij}) = \begin{cases} \infty & (r_{ij} < \sigma) \\ 0 & (r_{ij} > \sigma), \end{cases} \quad (2)$$

where σ is the diameter of the spherical patchy particles. $U_{\text{rep}}(r_{ij})$ represents the dependence of the attractive interaction on the distance between two particles, given by a square-well potential as

$$U_{\text{SW}}(r_{ij}) = \begin{cases} -\epsilon & (\sigma < r_{ij} < \sigma + \Delta) \\ 0 & (r_{ij} > \sigma + \Delta), \end{cases} \quad (3)$$

where Δ and ϵ are the width and depth of the attractive potential, respectively. $f(\hat{\mathbf{r}}_{ij}, \hat{\mathbf{n}}_i, \hat{\mathbf{n}}_j)$ in Eq. (1) represents anisotropy in the attractive interaction, making attraction occur only between the same types of patch. $f(\hat{\mathbf{r}}_{ij}, \hat{\mathbf{n}}_i, \hat{\mathbf{n}}_j)$ is given by

$$f(\hat{\mathbf{r}}_{ij}, \hat{\mathbf{n}}_i, \hat{\mathbf{n}}_j) = \begin{cases} 1 & \hat{\mathbf{n}}_i \cdot \hat{\mathbf{r}}_{ij} \geq \alpha \text{ and } \hat{\mathbf{n}}_j \cdot \hat{\mathbf{r}}_{ji} \geq \alpha, \text{ or } \hat{\mathbf{n}}_i \cdot \hat{\mathbf{r}}_{ij} \leq \beta \text{ and } \hat{\mathbf{n}}_j \cdot \hat{\mathbf{r}}_{ji} \leq \beta \\ 0 & \text{otherwise} \end{cases}, \quad (4)$$

where $\alpha = \cos \delta_A$ and $\beta = -\cos \delta_B$. To examine the effect of patch sizes on structures, the two angles δ_A and δ_B are controlled in simulations because these angles are related to the

areas of patches A and B as $\pi\sigma^2(1 - \cos \delta_A)/2$ and $\pi\sigma^2(1 - \cos \delta_B)/2$, respectively.

Simulation settings In isothermal-isobaric Monte Carlo simulations, the number of particles N is set to 1024. Focusing on the short interaction length, Δ was set to 0.1σ . Interaction strength is assumed to be large when compared with temperature, and $\epsilon/k_B T = 8, 6, \text{ or } 4$, where k_B is the Boltzmann constant and T is temperature.

Initially, particle positions and particle orientations are set at random. The initial system size is large enough for the system's volume to decrease in early stages of simulations. Two-dimensional translation of particle positions followed by three-dimensional rotation of particles is performed for each particle. In the three-dimensional rotation, the rotation for the vertical meridian and for the horizontal meridian are performed at the same time with neglecting the effect of the bottom wall. After the above trials are performed for all the particles, the effect of changing system size is investigated. These successive trials are performed 4×10^7 times. To avoid the accept ratios being too small or too large, the amplitudes of transition, rotation, and system size change are tuned every 400 times trials. The accept ratios of these trials are kept close to 0.5 during simulations.

Results and Discussion

Considering the symmetry of patchy particles, simulations are performed only for $\delta_A \geq \delta_B$. After typical structures and their structural units observed in simulations are illustrated, the lowest energy structures are summarized and compared with the results of simulations. The effect of neglecting the attractive interaction between different types of patches is also noted.

Typical structures observed in simulations

Figure 2 shows snapshots of typical structures obtained in simulations and zoomed snapshots for the areas surrounded by circles for several δ_A and δ_B . In these figures, the unit normal

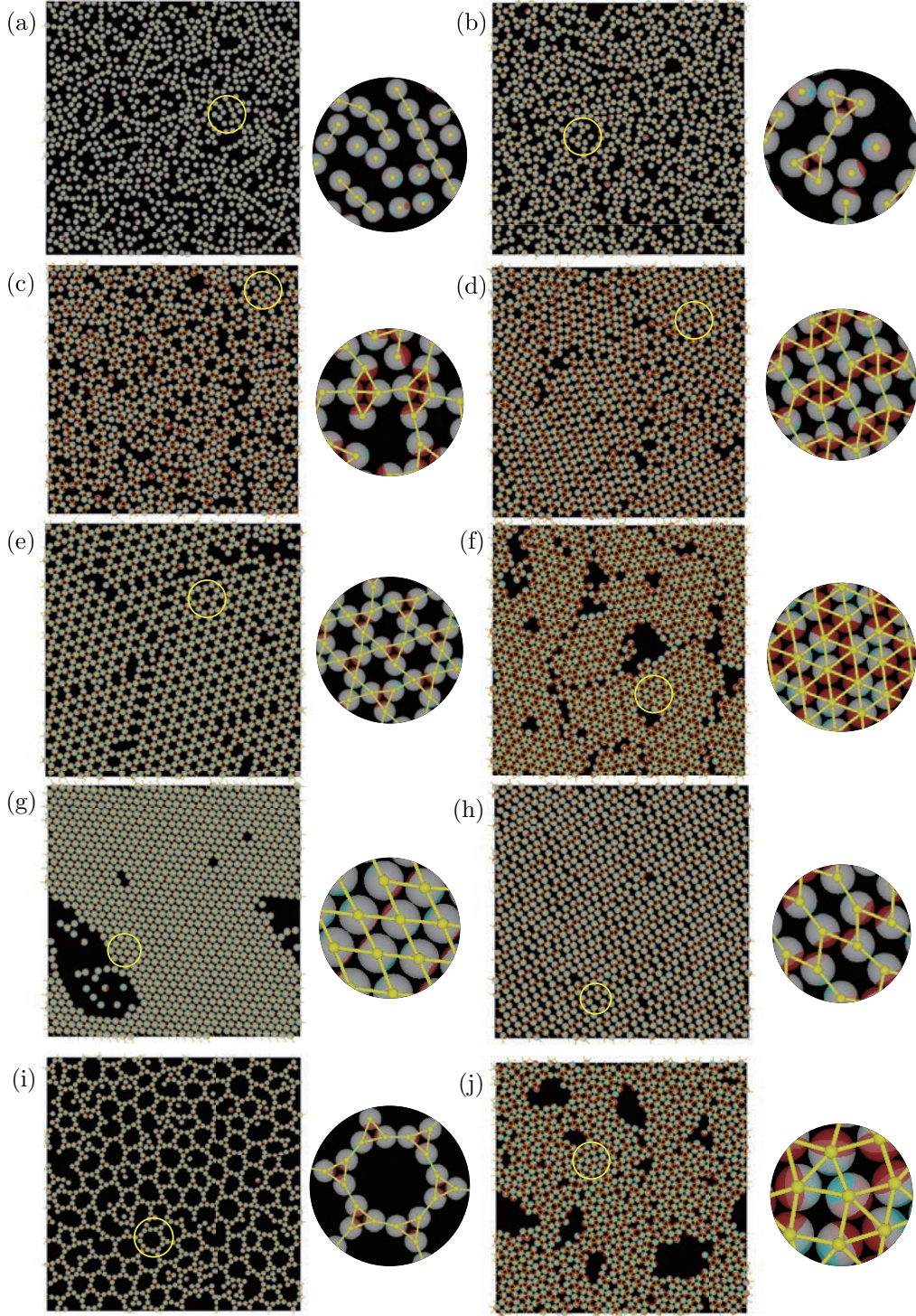


Figure 2: Snapshots of systems for $(\delta_A, \delta_B) =$ (a) $(20^\circ, 20^\circ)$, (b) $(45^\circ, 20^\circ)$, (c) $(70^\circ, 20^\circ)$, (d) $(80^\circ, 30^\circ)$, (e) $(50^\circ, 35^\circ)$, (f) $(90^\circ, 35^\circ)$, (g) $(35^\circ, 35^\circ)$, (h) $(60^\circ, 30^\circ)$, (i) $(45^\circ, 25^\circ)$, and (j) $(80^\circ, 50^\circ)$, Zoomed images for the circles areas are shown to right for each system snapshot. The pressure is set to $P\sigma^3/k_B T = 1.5$ from (a) to (g), (h) 2.0, (i) 0.5, and (j) 0.5. The interaction energy is set to $\epsilon/k_B T = 6.0$ from (a) to (h), and 8.0 for (j) and (h). Yellow lines show attraction between particles.

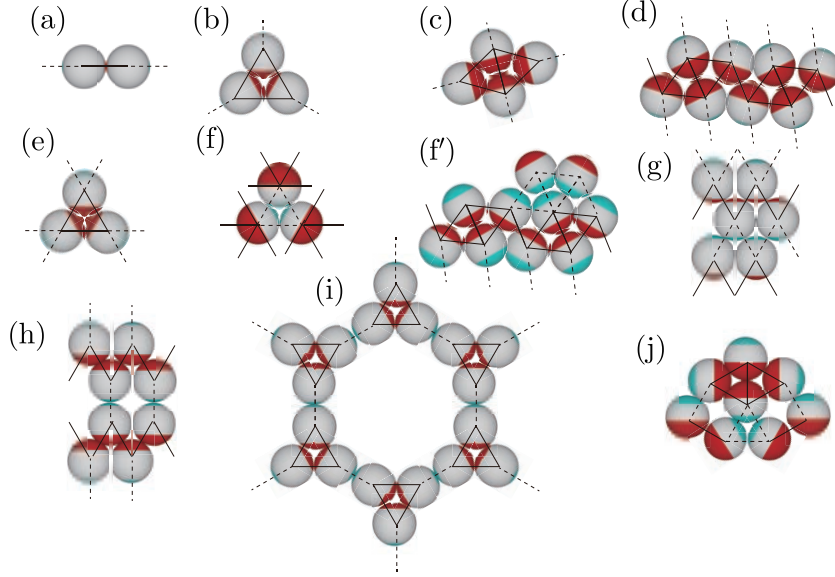


Figure 3: Ideal structural units shown in Fig. 2. (δ_A, δ_B) is (a) $(20^\circ, 20^\circ)$, (b) $(45^\circ, 20^\circ)$, (c) $(70^\circ, 20^\circ)$, (d) $(80^\circ, 30^\circ)$, (e) $(50^\circ, 35^\circ)$, (f) $(90^\circ, 35^\circ)$, (g) $(35^\circ, 35^\circ)$, (h) $(60^\circ, 30^\circ)$, (i) $(25^\circ, 45^\circ)$, and (j) $(80^\circ, 50^\circ)$. (f') shows another hexagonal structure created with $\delta_A = 60^\circ$ and $\delta_B = 60^\circ$. The connections at patch A are shown by solid lines and those at patch B with dotted lines.

vector of patch direction \mathbf{n}_i is almost parallel to the xy -plane, which is reasonable to increase attraction between patches. Thus, when considering ideal shapes of structural units (Fig. 3), I assume that the patch direction is parallel to the xy -plane.

Small clusters and structures by their connection Figure 2a shows a snapshot for $\delta_A = \delta_B = 20^\circ$. Straight chain-like clusters are created because both patch A and patch B are too small for two particles to attach to each patch. The structural unit is a dimer, as shown in Fig. 3(a). Because the numbers of particles attaching to patch A and patch B are at most $n_A = 1$ and $n_B = 1$, respectively, the total number of particles attaching to a particle was $n = 2$ at maximum. The structural unit, the dimer, is able to be created for $\delta_A \geq 0$ and $\delta_B \geq 0$. If the straight chain-like structure is created by the connection of dimers, the energy gain per particle, $\Delta\epsilon$, is $-\epsilon$.

To examine what structures are created when increasing the difference in patch sizes, simulations are performed for larger δ_A , setting δ_B to be 20° . Figure 2b shows a snapshot

for $\delta_A = 45^\circ$ and $\delta_B = 20^\circ$. Because δ_A exceeds 30° , two particles are able to attach to patch A and triangular trimers such as Fig. 3b are created. The trimers are able to connect to other triangular trimers at patch B, allowing formation of heximers (as shown in the zoomed snapshot) and other larger clusters. The structural unit, the triangular trimer, can be created when $\delta_A > 30^\circ$ and $\delta_B \geq 0$. $n_A = 2$ and $n_B = 1$ because the area of patch B is small, so that $n = 3$ and $\Delta\epsilon = -3\epsilon/2$ if all the bonds are connected.

For $\delta_a = 70^\circ$ and $\delta_B = 20^\circ$ (Fig. 2c), the structural unit is a rhomboidal tetramer, as shown in Fig. 3(c). The structural units are able to be created when $\delta_A > 60^\circ$ and $\delta_B \geq 0^\circ$. These rhomboidal tetramers connect to each other at patch B, as shown in a zoomed snapshot. In structural units, $n_A = 3$ and $n_B = 1$ for two particles and $n_A = 2$ and $n_B = 1$ for the other two particles, the average value of the interacting particles per particle is $n = 3.5$ and $\Delta\epsilon = -7\epsilon/4$.

When $\delta_A > 60^\circ$ and $\delta_B \geq 0^\circ$ zigzag chain-like clusters including rhomboids,^{9,30} are also created as shown in Fig. 2d. The zigzag chains are able to connect with each other at patch B if $\delta_B \geq 60^\circ - \delta_A$ as shown in Fig. 3d. In Fig. 2d, parallel zigzag chains are connected because two angles satisfy the condition. In the structure, $n_A = n_B = 2$ as shown in Fig, 2c. Because $n = 4$ and $\Delta\epsilon = -2\epsilon$, $\Delta\epsilon$ is larger than that for the connection of rhomboidal tetramers.

Kagome lattice A kagome lattice, which also forms when patch A and patch B are the same, is created²⁷ when $\delta_A \geq 30^\circ$ and $\delta_B \geq 30^\circ$ (Fig. 2e). Because a triangular trimer such as Fig 3e becomes the structural unit, the form of the unit is the same as Fig 3b. However, the number of attachable particles per patch is different between the two cases. $n_A = 2$ for both units, but $n_B = 1$ for Fig 3b and $n_B = 2$ for Fig 3e. Because $n = 4$ and $\Delta\epsilon = -2\epsilon$ for Fig 3e and $n = 3$ and $\Delta\epsilon = -3\epsilon/2$ for Fig. 3b, the kagome lattice is more stable than the connection of triangular tetramers (Fig. 3b). $\Delta\epsilon$ for the formation of a kagome lattice is the same as $\Delta\epsilon$ for the formation of zigzag chains (Fig. 3d), but n_A and n_B are different. Because $n_A = 3$ and $n_B = 1$ in Fig 3c, the connection between patch B for the zigzag chains

is weaker than that for the kagome lattice for thermal fluctuations.

Hexagonal structures When $\delta_B \geq 30^\circ$ and $\delta_A \geq 90^\circ$, the formation of a hexagonal lattice is possible. Fig. 2f shows a snapshot for $\delta_A = 90^\circ$ and $\delta_B = 35^\circ$. Because δ_B is close to the critical value, the unit of this structure is a triangular trimer such as Fig 3f, in which particles are connected at patch B. When the hexagonal lattice is created by the ideal triangular trimers, zigzag chains can be created by the connection of particles at patch A, which is located outside of the trimers as observed in the zoomed snapshot in Fig. 2f. Because $n_A = 4$ and $n_B = 2$, $n = 6$ and $\Delta\epsilon = -3\epsilon$. The formation of another type of hexagonal lattice is possible when δ_B is increased. In the hexagonal lattice, the zigzag connections including rhomboidal units are created for both patches A and B (Fig. 3d). This structure can be created when $\delta_B \geq 60^\circ$ and $\delta_A \geq 60^\circ$. $\Delta\epsilon$ in the hexagonal structure is the same as that in Fig 3f.

Figure 2g shows the hexagonal lattice for $\delta_A = 35^\circ$ and $\delta_B = 35^\circ$, which is different from the two hexagonal lattices mentioned above. The formation of this type of hexagonal lattice is possible when $\delta_A > 30^\circ$ and $\delta_B > 30^\circ$. As shown in Fig. 3g, patch A is parallel for all particles. For both patch A and patch B, zigzag chains not including rhomboids are created. Because $n_A = n_B = 2$, $n = 4$ and $\Delta\epsilon = -2\epsilon$. Thus, this hexagonal lattice is likely to be less stable against thermal fluctuations than the other two hexagonal lattices.

Deformed honeycomb structure and ring-like structure When δ_B is smaller than 30° , the zigzag chain created by patch B becomes impossible. The connections are broken into the connections of two particles as shown in Fig 3h. However, the zigzag connections created by patch A still remain, so that a deformed honeycomb lattice shown in Fig. 3h is created. For Fig 2h, δ_B is just the critical value 30° , so that δ_B is not large enough for the connection to be stable against thermal fluctuations. Thus, the honeycomb lattice is created as shown in the zoomed snapshot. In this structure, $n_A = 2$ and $n_B = 1$, so that $n = 3$ and $\Delta\epsilon = -3\epsilon/2$.

Because the formation of triangular trimers such as Fig. 3b is more stable at low pressure,¹¹ the pressure for creation of a deformed honeycomb structure satisfies $P\sigma^3/k_B T = 2.0$, which is larger than $P\sigma^3/k_B T = 1.5$ for Fig. 3b. With the pressure, triangular trimers are connected and small clusters are created as shown in Fig. 2b. When the pressure is much lower and the interaction energy is larger, a regular and sparser structure is created with triangular trimers. Figure 2i shows a snapshot of the sparser structure created with $\delta_A = 35^\circ$ and $\delta_B = 25^\circ$, where the interaction energy and pressure are given by $\epsilon/k_B T = 8.0$ and $P\sigma^3/k_B T = 0.5$, respectively. A triangular trimer, such as Fig. 3b, is the structural unit of this structure because δ_A exceeds 30° , and a mesh-like sparse structure consisting of rings^{17,29,34} is created. In Fig 2i, twelve-membered rings are dominant because δ_B is small. If δ_B becomes larger, the connection of trimers at patch B can be more flexible and different-membered rings may be created. For the system, the formation of odd membered rings²⁵ are also possible because the patches on the outside of trimers, which are the growth units, are the same type, patch B. The range of δ_A and δ_B for creating the sparse structure is the same as that for the deformed honeycomb structure, $\delta_A \geq 30$ and $\delta_B \geq 0$. In the structure, $n_A = 2$ and $n_B = 1$, so that $n = 3$ and $\Delta\epsilon = -3\epsilon/2$.

Dodecagonal quasi-crystal structure Figure 2j shows a structure with $\delta_A = 80^\circ$ and $\delta_B = 50^\circ$. The structure is highly disordered with no apparent regularity. However, σ environments consisting of square tiles and triangular tiles (Fig. 4e) are observed, as shown in the zoomed snapshot. σ environments shown in Fig. 3j are created when $\delta_A \geq 60^\circ$ and $\delta_B \geq 30^\circ$. For the centered particle in the σ environment, $n_A = 3$ and $n_B = 2$, so that $n = 5$ and $\Delta\epsilon = -5\epsilon/2$ for the structure.

Because the formation of a σ environment may imply that the structure is a two-dimensional dodecagonal quasi-crystal,³⁵⁻³⁷ detailed properties of the system are examined to clarify whether the structure obtained in the simulation is a two-dimensional dodecagonal quasi-crystal or not. As criteria for judging the formation of two-dimensional dodecagonal

quasi-crystal, the static structure factor $S(\mathbf{q})$ and the local rotational order ϕ_m are calculated. These two parameters are defined as follows:

$$S(\mathbf{q}) = \frac{1}{N} \sum_i \sum_j \exp(2\pi i \mathbf{q} \cdot (\mathbf{r}_i - \mathbf{r}_j)), \quad (5)$$

$$\phi_m(i) = \frac{1}{n_i} \left| \sum_j \exp(im\theta_{ij}) \right|, \quad (6)$$

where n_i is the number of neighboring particles for the i th particle and θ_{ij} represents the angle between \mathbf{r}_{ij} and the x -axis. When calculating the local m -fold rotational order for the i th particle $\phi_m(i)$, summation is performed only for the neighboring particles. The j th particle is regarded as a neighboring particle when r_{ij} is smaller than the critical value r_c , which is set to 1.2σ in the following analyses.

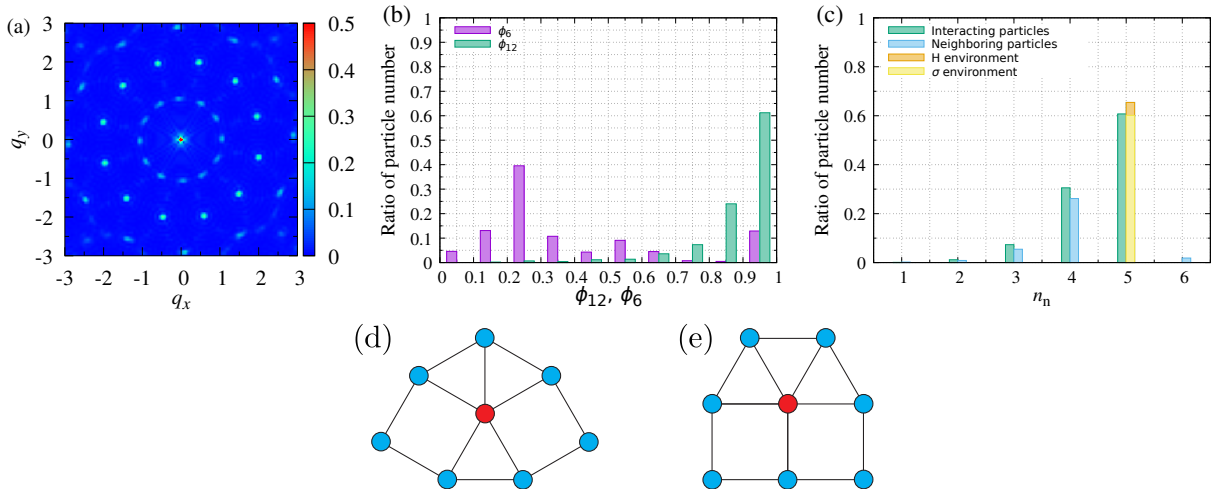


Figure 4: (a) $|S(\mathbf{q})/S(\mathbf{0})|$, (b) distribution of the order parameters ϕ_6 and ϕ_{12} , and (c) distribution of numbers of interacting particles n_I and that of neighboring particles for the system shown n_N . For $n_N = 5$, the numbers of σ environments and H environments are shown. Data for Fig. 2j is used in these figures. Red particles in (d) and (e) indicate the particles in the σ environment and the H environment, respectively.

Figure 4(a) shows $|S(\mathbf{q})/S(\mathbf{0})|$ for Fig. 2j. Sharp bright spots appear around $(q_x, q_y) = (0, 0)$, indicating that the structure has the long-range order with the twelve-fold rotational symmetry. Figure 4(b) shows the distribution of ϕ_6 and ϕ_{12} for Fig. 2j, where the y -axis

is normalized by the total particle number in the system N . For most particles, ϕ_{12} is larger than 0.7.²⁷ Both ϕ_{12} and ϕ_6 are high if the hexagonal lattice is created, but ϕ_6 is small for many particles, so that a hexagonal structure is not created. Figure 4c shows the distribution of the numbers of neighboring particles n_N and that of interacting particles n_I . The distributions of n_N and n_I are almost the same except that a few particles with $n_N = 6$ appear for n_I . The number of particles with $n_N = 5$ is the most numerous in the system, which is consistent with the formation of a two-dimensional dodecagonal quasi-crystal. With $n_N = 5$ and high ϕ_{12} , particles in H environments (Fig. 4e) are also possible, prompting examination of the ratio of σ environments to H environments for the particles with $n_N = 5$. For particles with $n_N = 5$, the number of the particles in σ environments is 616 of 670 particles, causing approximately 90% of the particles with $n_N = 5$ to exist in σ environments, with the residuals existing in H environments. Considering that δ_A should be equal to or exceed 90° for creating H environments, it is reasonable that few H environments are created in Fig. 2j. From these results, the structure shown in Fig 2j is judged as a two-dimensional dodecagonal quasi-crystal.

Dependence of structures on the patch areas

Here, I show the dependence of structures on the two patch areas, as expected from $\Delta\epsilon$, and compare this with the simulation results, indicating the relationship between structures and the two patch areas obtained from simulations, were indicated. The effect of neglecting the attractive interaction between two different patches on the structure is also briefly discussed.

Relationship between structures predicted from $\Delta\epsilon$ and two angles

Figure 5 shows how the relationship between the structures observed in the simulations and two patch angles is expected from $\Delta\epsilon$. The number of interacting particles is counted to determine which structure is the most stable, because $\Delta\epsilon$ is proportional to the number of interacting particles. When $0^\circ < \delta_A \leq 30^\circ$ and $0^\circ < \delta_B \leq 30^\circ$, the straight-chain structure is expected,

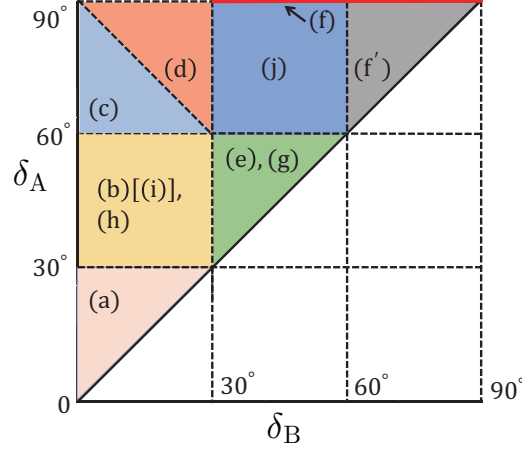


Figure 5: Dependence of the structures and their units observed in the simulations on δ_A and δ_B , which are expected from the interaction energy. In the figure, (a) to (j) indicate the ideal units in Fig. 3(a) to (j), respectively.

formed by Fig. 3a, where $n = 2$ if all possible bonding is connected.

When $30^\circ \leq \delta_A \leq 60^\circ$ and $0^\circ \leq \delta_B \leq 30^\circ$, the connection of triangular trimers (Fig. 3b) or honeycomb structure (Fig. 3c) are created. A twelve-membered ring-like structure,³⁴ as shown in Fig. 3i, is created by the connection of triangular trimers, and acts as the unit of the mesh-like structure shown in Fig. 2i. The structure is created when the pressure is low and the interaction energy ϵ is large. In the region, the expected number of interacting particles is $n = 3$ for all these structures.

For $60^\circ \leq \delta_A$ and $\delta_A \leq 60^\circ - \delta_B$, the rhomboidal tetramer (Fig. 3c) formed as the structural unit, and they were connected at patch B. Because there are particles with $n = 3$ and $n = 4$ with the same ratio, the average number of interacting particles is $n = 3.5$. When $\delta_A \geq 60^\circ - \delta_B$ and $\delta_B \leq 30^\circ$, zigzag chains form, connected by patch A. In the zigzag chains, the rhomboidal structure is included, and the chains are able to attach to each others via patch B, as shown Fig. 3d. In the region, the expected number of interacting particles is $n = 4$ for the structure.

For $60^\circ \leq \delta_A \leq 90^\circ$ and $30^\circ \leq \delta_B \leq 60^\circ$, a structure with square tiles and triangular tiles is created (Fig. 3j), where the formation of two-dimensional dodecagonal quasi-crystal is possible. In this region, the expected number of interacting particles is $n = 5$. The kagome

lattice²⁷ forms when $30^\circ \leq \delta_A \leq 60^\circ$ and $30^\circ \leq \delta_B \leq 60^\circ$ (Fig. 3e). In the above region, a hexagonal structure with the same n is also created. In the hexagonal structure, patch A and patch B create the zigzag chains (Fig. 3g), with an expected number of interacting particles is $n = 4$ in the region. Other two types of hexagonal structures are observed in the simulations, with one in which both patch A and B create a zigzag of rhomboids (Fig. 3f'). This structure is created for $\delta_A \geq 60^\circ$ and $\delta_B > 60^\circ$. The other hexagonal structure, which was shown in Fig. 3f, is possible when $\delta_A = 90^\circ$ and $\delta_B > 60^\circ$. $n = 6$ for these two structures, causing them to both be more stable than the first hexagonal structure.

Dependence of structures on δ_A and δ_B obtained from simulations To indicate whether the structures observed in simulations agree with Fig. 5 or not, I examine the average number of interacting particles obtained.

Figure 6 shows the average number of interacting particles obtained from the simulations. For $\epsilon/k_B T = 6.0$ and $P\sigma^3/k_B T = 2.0$ (Fig 6c), the result agrees with Fig. 5 except for the region with $60^\circ \leq \delta_A \leq 90^\circ$ and $0^\circ \leq \delta_B \leq 30^\circ$. In this region, the connection of rhomboidal clusters or the connection of the zigzag chain of rhomboids is possible as shown in Fig. 5. Because $n = 3.5$ for the connection of rhomboidal clusters and $n = 4$ for the connection of the zigzag chain of rhomboids, the two structures are not distinguished in the color difference used in this figure if the large clusters are created. Considering this ambiguity, the result is reasonable.

With a smaller $P\sigma^3/k_B T$ (Figs. 6a and 6b), the average number of interacting particles becomes smaller than that expected from Fig. 5 when δ_A and δ_B are small, meaning that ϵ used in Figs. 6a and 6b is not large enough to create the large cluster.

For $\epsilon/k_B T = 8.0$ (Fig 6d, 6e, and 6f), the average number of interacting particles agrees well with Fig. 5 in almost of all the regions except for the region (f) in Fig. 5. Because a hexagonal lattice is expected in the region, n should be $5 \leq n \leq 6$. However, the number of interacting particles is smaller than the expected value, which is probably due to the

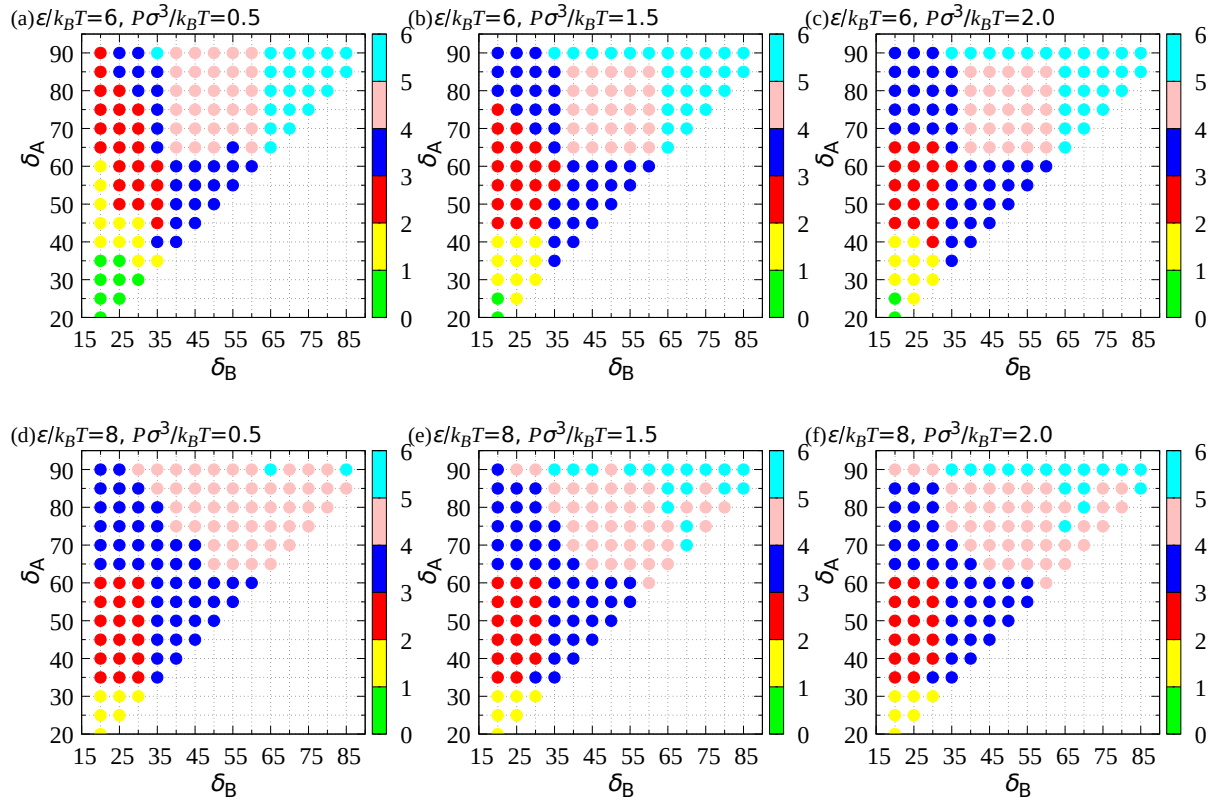


Figure 6: Distribution of the average number of interacting particles per particle for $(\epsilon/k_B T, P\sigma^3/k_B T) =$ (a) (6, 0.5), (b) (6, 1.5), (c) (6, 2.0), (d) (8, 0.5), (e) (8, 1.5), and (f) (8, 2.0).

creation of large vacancies in the lattice; once vacancies are created, they remain stably against thermal fluctuations because of a large interaction energy.

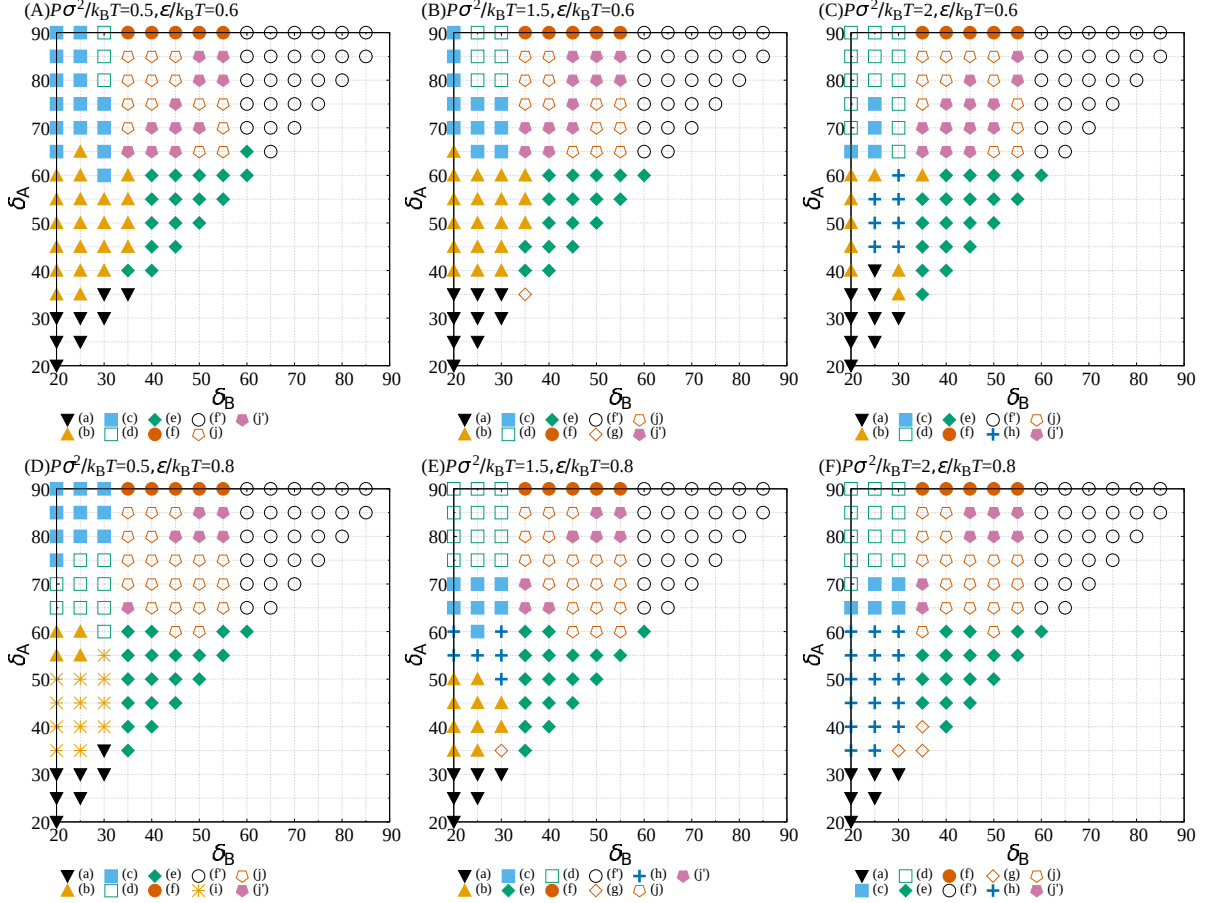


Figure 7: Distribution of the average number of interacting particles per particle for $(\epsilon/k_B T, P\sigma^3/k_B T) =$ (A) (6, 0.5), (B) (6, 1.5), (C) (6, 2.0), (D) (8, 0.5), (E) (8, 1.5), and (F) (8, 2.0). (a) to (j) in these figures indicate the same structures as in Fig. 3(a) to (j) and (j') shows the two-dimensional dodecagonal quasi-crystal structure.

Dependence of dominant structures on δ_A and δ_B Figure 7 shows the dependence of the dominant structures obtained from the simulations on δ_A and δ_B . The dominant structures are determined with Fig. 6 and the snapshots. For the hexagonal lattices, such as Figs 3f and 3f' the parameter regions agree well with Fig. 5. The region with these structures shows little dependence on $\epsilon/k_B T$ and $p\sigma^3/k_B T$. For the structure created by square tiles and triangular tiles, the structure factor $S(\mathbf{q})$ and the order parameters for local rotational symmetry, ϕ_{12} and ϕ_6 , are examined to determine whether the dodecagonal quasi-crystal

structure is created or not. The dodecagonal quasi-crystal structure tends to form mainly around $\delta_A = 65^\circ$ and $\delta_B = 35^\circ$, or $\delta_A = 85^\circ$ and $\delta_B = 55^\circ$.

The hexagonal lattice shown in Fig. 3g is created in a narrow parameter region when $P\sigma^3/k_B T = 1.5$ and 2.0. Instead, the kagome lattice tends to form with the same energy as the hexagonal lattice but with a sparser structure. In higher pressure simulations, the hexagonal structure becomes dominant, with a larger parameter region, because of closer structure.

In the region where triangular trimers such as Fig 3b or honeycomb structures such as Fig 3h are possible, the honeycomb structure is created at high pressure (Fig 7C and 7F) because the particle density is able to be higher than that in the structure created with triangular trimers. At low pressure (Fig 7D), the formation of sparse structures is possible, and a mesh-like structure composed of twelve-membered ring-like structure such as Fig 3i forms as a regular structure created with triangular trimers (Fig 3b). With other parameters (Fig 7A, 7B, and 7E), a chain-like structure is caused, caused by the connection of triangular trimers were created in the region.

Effect of neglecting the attraction between two different patches In our model, the attraction only exists between the same type of patches, and neglecting the attraction between the different type of patches is important for creating certain structures.

Figure 8 shows snapshots of structures with the attraction between the different types of patches. For $\delta_A = 45^\circ$ and $\delta_B = 25^\circ$, the mesh-like structure, composed of the twelve-membered ring-like structural units, is created when the attraction between the different types of patches is neglected, but in Fig. 8a, the mesh-like structure is more disordered than that in Fig. 2i because the size of the ring-like structure is irregular. For $\delta_A = 80^\circ$ and $\delta_B = 30^\circ$, the zigzag chain including rhomboids is formed without the attraction between the different types of patch (Fig. 2d). However, the zigzag chain-like structure is not formed, and the structures created with square connections and triangular connections form, instead

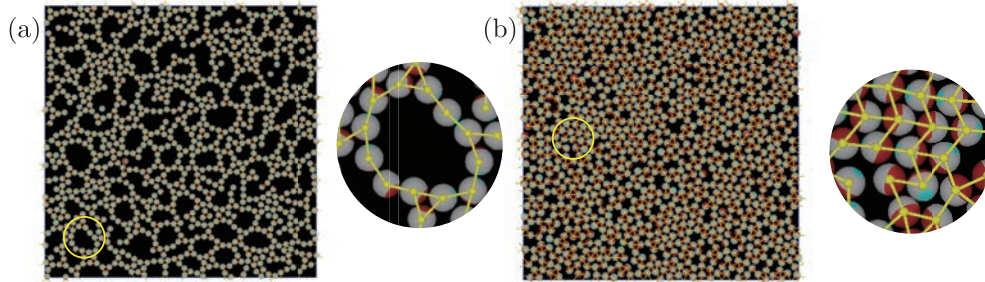


Figure 8: Snapshots showing the interaction between different types of patches for $(\delta_A, \delta_B) =$ (a) $(45^\circ, 25^\circ)$ and (b) $(80^\circ, 30^\circ)$, where $P\sigma^3/k_B T$ and $\epsilon/k_B T$ in Fig. reffig:with-different-patches (a) and (b) are the same as those in Fig. 2i and 2d, respectively .

(Fig. 8b). The changes in these structures are due to the increase in irregularity caused by the connection of patches A and B in the zoomed snapshots. In experiments,^{29,30} the twelve-membered ring-like structures and zigzag chain-like structures are observed in the system with attraction between the different types of patch, but these structures may be created more regularly when the two different patches do not attract each other.

Conclusion

In this paper, I performed isothermal-isobaric Monte Carlo simulations and examined the two-dimensional structures formed by triblock patchy particles with two different patches under assumption that the same type of patches attract each other. When changing the patch areas, various structures such as a ring-like structure,^{17,34} zigzag-chain structure, kagome lattice,²⁷ and dodecagonal quasi-crystal structure³⁵⁻³⁷ are created. In the simulations, the interaction energy was set to $\epsilon/k_B T = 8.0$ or 6.0 . Experiments have been performed with the interaction energy $\epsilon/k_B T \leq 10$,²⁷ so the interaction energy in these simulations is in a feasible region. In our simulations, the different types of patches were assumed not to interact with each other. These types of patches may be created when DNA-coated colloidal particles are used.^{19,38-50} Because DNA strands are easy to design according to a purpose,

the required interaction can be possible when two types of DNA strands, which interact with the same type of DNA strands, are attached to the two different patches.

Even if the different patches are able to interact with each other, the ring-like structure and zigzag chain-like structures are created by interaction between disparate patch sizes. However, the regularity of these structures is improved if the different patches do not attract each other, because the structural units such as triangular trimers are created more uniformly. Therefore, controlling the interaction between two different patches is effective for creating these complicated regular structures.

The dodecagonal quasi-crystal structure is also created in a system where particles have five or more patches.³⁵⁻³⁷ In this study, I show that this quasi-crystal structure can be created in a much simpler system, in which patchy particles have only two patches, and is created when the triangular tiles and square tiles are able to form. However, the quasi-crystal is not necessarily created when these tiles are present, and the exact formation conditions of the quasi-crystal structure have not been determined. Clarifying these formation conditions is an open problem to be addressed in future work. Although only primitive analyses are performed in this paper, more quantitative characterizations are possible using other methods.⁵¹⁻⁵⁶ For example, for the parameter region where straight chain-like clusters are created, the cluster classification algorithms used by Lotito et al.⁵⁵ may be useful. For the analysis regarding rhomboidal structures and the distinction of H and σ environments, voronoi tessellation and shape factor analysis could be helpful.^{51,52,54} By using these methods, the structures observed in my simulations may be classified and quantified more clearly. In this paper, I just examine how the dominant structure depends on parameters, but I should have examined the phase diagram²¹ to clarify properties of structures, which is also one of our future problems.

Acknowledgement

This work was supported by JSPS KAKENHI, Grant nos. JP20K03782 and 21K04908,

and the Grant for Joint Research Program of the Institute of Low Temperature Science, Hokkaido University, Grant no. 22G015. Thanks to M. Hammonds PhD, from Edanz (<https://jp.edanz.com/ac>) for editing a draft of this manuscript.

References

- (1) Maldovan, M.; Ullal, C. K.; Carter, W. C.; Thomas, E. L. Exploring for 3D Photonic Bandgap Structures in the 11 F.C.C. Space Groups. *Nat. Mater.* **2003**, 2, 664-667.
- (2) Hynninen, A.-P.; Thijssen, J. H. J.; Vermolen, E. C. M.; Dijkstra, M.; van Blaaderen, A. Self-Assembly Route for Photonic Crystals with a Bandgap in the Visible Region. *Nat. Mater.* **2007**, 6, 202-205.
- (3) von Freymann, G.; Kitaev, V.; Lotsch, B. V.; Ozin, G. A. Bottom-Up Assembly of Photonic Crystals. *Chem. Soc. Rev.* **2013**, 42, 2528-2554.
- (4) Joannopoulos, J. D.; Villeneuve, P. R.; Fan, S. Photonic Crystals: Putting a New Twist on Light. *Nature* **1997**, 386, 143-149.
- (5) Ho, K. M.; Chan, C. T.; Soukoulis, C. M. Existence of a Photonic Gap in Periodic Dielectric Structures. *Phys. Rev. Lett.* **1990**, 65, 3152-3155.
- (6) Ngo, T. T.; Liddell, C. M.; Ghebrebrhan, M.; Joannopoulos, J. D. Tetrastack: Colloidal Diamond-Inspired Structure with Omnidirectional Photonic Band Gap for Low Refractive Index Contrast. *Appl. Phys. Lett.* **2006**, 88, 241920.
- (7) Preisler, Z.; Vissers, T.; Smalenburg, F.; Munaò, G.; Sciortino, F. Phase Diagram of One-Patch Colloids Forming Tubes and Lamellae. *J. Phys. Chem. B* **2013**, 117, 9540-9547.
- (8) Vissers, T.; Preisler, Z.; Smalenburg, F.; Dijkstra, M.; Sciortino, F. Predicting crystals of Janus colloids. *J. Chem. Phys.* **2013**, 138, 164505.

- (9) Iwashita, Y.; Kimura, Y. Stable cluster phase of Janus particles in two dimensions. *Soft Matter* **2013**, 9, 10694-10698.
- (10) Vissers, T.; Smallenburg, F.; Munaò, G.; Preisler, Z.; Sciortino, F. Cooperative polymerization of one-patch colloids. *J. Chem. Phys.* **2014**, 140, 144902.
- (11) Shin, H.; Schweizer, K. S. Theory of two-dimensional self-assembly of Janus colloids: crystallization and orientational ordering. *Soft Matter* **2014**, 10, 262-274.
- (12) Preisler, Z.; Vissers, T.; Munaò, G.; Smallenburg, F.; Sciortino, F. Equilibrium phases of one-patch colloids with short-range attractions. *Soft Matter* **2014**, 10, 5121-5128.
- (13) Iwashita, Y.; Kimura, Y. Spatial confinement governs orientational order in patchy particles. *Sci. Rep.* **2016**, 6, 27599.
- (14) Preisler, Z.; Vissers, T.; Smallenburg, F.; Sciortino, F. Crystals of Janus colloids at various interaction ranges. *J. Chem. Phys.* **2016**, 145, 064513.
- (15) Iwashita, Y.; Kimura, Y. Density dependence of orientational order in one-patch particles. *Soft Matter* **2017**, 13, 4997-5007.
- (16) Cerbelaud, M.; Lebdioua, K.; Tran, C. T.; Crespín, B.; Aimablea, A.; Videcoqa, A. Brownian dynamics simulations of one-patch inverse patchy particles. *Phys. Chem. Chem. Phys.* **2019**, 21, 23447-23458.
- (17) Oh, J. S.; Lee, S.; Glotzer, S. C.; Yi, G.-R.; Pine, D. J. Colloidal fibers and rings by cooperative assembly. *Nat. Commun.* **2019**, 10, 3936.
- (18) Sato, M. Self-Assembly Formed by Spherical Patchy Particles with Long-Range Attraction. *J. Phys. Soc. Jpn* **2019**, 88, 104801.
- (19) Oh, J. S.; Yi, G.-R.; Pine, D. J. Reconfigurable Transitions between One- and Two-Dimensional Structures with Bifunctional DNA-Coated Janus Colloids *ACS Nano* **2020**, 14, 15786-15792.

- (20) Sato, M. Effect of Patch Area and Interaction Length on Clusters and Structures Formed by One-Patch Particles in Thin Systems *ACS Omega* **2020**, 5, 28812-28822
- (21) Reinhart, W. F.; Panagiotopoulos, A. Z. Equilibrium crystal phases of triblock Janus colloids. *J. Chem. Phys.* **2016**, 145, 094505.
- (22) Reinhart, W. F.; Panagiotopoulos, A. Z. Crystal growth kinetics of triblock Janus colloids. *J. Chem. Phys.* **2012**, 136, 054904.
- (23) Morphew, D.; Shaw, J.; Chakrabarti, D. Programming Hierarchical Self-Assembly of Patchy Particles into Colloidal Crystals via Colloidal Molecules. *ACS Nano* **2018**, 12, 2355-2364.
- (24) Rao, A. B.; Shaw, J.; Neophytou, A.; Morphew, D.; Sciortino, F.; Jhonston, R. L.; Chakrabarti, D.; Leveraging Hierarchical Self-Assembly Pathways for Realizing Colloidal Photonic Crystals. *ACS Nano* **2020**, 14, 5348-5359.
- (25) Neophytou, A.; Manoharan, V. N.; Chakrabarti, D. Self-Assembly of Patchy Colloidal Rods into Photonic Crystals Robust to Stacking Faults. *ACS Nano* **2021**, 15, 2668-2678.
- (26) Neophytou, A.; Chakrabarti, D.; Sciortino, F. Topological nature of the liquid-liquid phase transition in tetrahedral liquids. *Nat. Phys.* **2022**, 18, 1248-1253.
- (27) Chen, Q.; Bae, S. C.; Granick S. Directed self-assembly of a colloidal kagome lattice. *Nature* **2011**, 469, 382-385.
- (28) Romano, F.; Sciortino, F. Patchy from the bottom up. *Nature Mater.* **2011**, 10, 171-173.
- (29) Chen, Q.; Diesel, E.; Whitmer, J. K.; Base, S. C.; Luijten, E.; Granick, S. Triblock Colloids for Directed Self-Assembly. *J. Am. Chem. Soc.* **2011**, 133, 7725-2227.
- (30) Chen, Q.; Yan, J.; Zhang, J.; Bae, S. C.; Granick, S. Janus and Multiblock Colloidal Particles. *Langmuir* **2012**, 28, 13555-13561

- (31) Mao, X.; Chen, Q.; Granick, S. Entropy favours open colloidal lattices. *Nat. Mat.* **2013**, 12, 217-222.
- (32) Bol, W. Monte Carlo simulations of fluid systems of waterlike molecules. *Mol. Phys.* **1982**, 45, 605-616.
- (33) Kern, N.; Frenkel, D. Fluid-fluid coexistence in colloidal systems with short-ranged strongly directional attraction. *J. Chem. Phys.* **2003**, 118, 9882-9889.
- (34) Lindquist, B. A.; Jadrich, R. B.; Truskett, T. M.; Inverse design for selfassembly via on-the-fly optimization *J. Chem. Phys.* **2016**, 145, 111101.
- (35) van der Linden, M. N.; P. K. Doye, J.; Louis, A. A. Formation of dodecagonal quasicrystals in two-dimensional systems of patchy particles. *J. Chem. Phys.* **2012**, 136, 054904.
- (36) Reinhardt, A.; Romano, F.; P K Doye, J. Computing Phase Diagrams for a Quasicrystal-Forming Patchy-Particle System. *Phys. Rev. Lett.* **2013**, 110, 255503.
- (37) Reinhardt, A.; Schreck, S. J.; Romano, F.; P K Doye, J. Self-assembly of two-dimensional binary quasicrystals: a possible route to a DNA quasicrystal *J. Phys.: Condens. Matter* **2017**, 29, 014006.
- (38) Mirkin, C. A.; Letsinger, R. L; Mucic, R. C.; Storhoff, J. J. A DNA-based method for rationally assembling nanoparticles into macroscopic materials *Nature* **1996**, 382, 607-609.
- (39) Nykypanchuk, D.; Maye, M. M.; van der Lelie, D. ; Gang, O. DNA-guided crystallization of colloidal nanoparticles. *Nature* **2008**, 451, 549-552.
- (40) Park, S. Y.; Lytton-Jean, A. K. R.; Lee, B.; Weigand, S.; Schatz, G. C.; Mirkin, C. A. DNA-programmable nanoparticle crystallization. *Nature* **2008**, 451, 553-556.

- (41) Xiong, H.; Lelie, D. v. d.; Gang O. Phase Behavior of Nanoparticles Assembled by DNA Linkers. *Phys. Rev. Lett.* **2009**, 102, 015504.
- (42) Macfarlane, R. J.; Lee, B.; Hill, H. D.; Senesi, A. J.; Seifert, S.; Mirkin, C. A. Assembly and organization processes in DNA-directed colloidal crystallization. *Proc. Natl. Acad. Sci. U.S.A.* **2009**, 106, 10493-10498.
- (43) Cigler, P.; Lytton-Jean, A. K. R.; Anderson, D. G.; Finn, M. G.; Park, S. Y. DNA-controlled assembly of a NaTl lattice structure from gold nanoparticles and protein nanoparticles. *Nat. Mater.* **2010**, 9, 918-922.
- (44) Macfarlane, R. J.; Lee, B.; Jones, M. R.; Harris, N.; Schatz, G. C.; Mirkin, C. A. Nanoparticle Superlattice Engineering with DNA. *Science* **2011**, 334, 204-208.
- (45) Knorowski, C.; Burleigh, S.; Travesset, A. Dynamics and Statics of DNA-Programmable Nanoparticle Self-Assembly and Crystallization. *Phys. Rev. Lett.* **2011**, 106, 215501.
- (46) Zhang, C.; Macfarlane, R. J.; Young, K. L.; Choi, C. H. J.; Hao, L.; Auyeung, E.; Liu, G.; Zhou, X.; Mirkin, C. A. A general approach to DNA-programmable atom equivalents. *Nat. Mater.* **2013**, 12, 741-746.
- (47) Li, T. I. N. G.; Sknepnek, R.; de la Cruz, M. O. Thermally Active Hybridization Drives the Crystallization of DNA-Functionalized Nanoparticles. *J. Am. Chem. Soc.* **2013**, 135, 8535-8541.
- (48) Di Michele, L.; Varrato, F.; Kotar, J.; Nathan, S. H.; Foffi, G.; Eiser, E. Multistep kinetic self-assembly of DNA-coated colloids. *Nat. Commun.* **2013**, 4, 2007.
- (49) Srivastava, S.; Nykypanchuk, D.; Fukuto, M.; Halverson, J. D.; Tkachenko, A. V.; Yager, K. G.; Gang, O. Two-Dimensional DNA-Programmable Assembly of Nanoparticles at Liquid Interfaces. *J. Am. Chem. Soc.* **2014**, 136, 8323-8332.

- (50) Wang, S.; Park, S. S.; Buru, C. T.; Lin, H.; Chen, P.-C.; Roth, E. W.; Farha, O. K.; Mirkin, C. A. Colloidal crystal engineering with metal-organic framework nanoparticles and DNA. *Nat. Commun.* **2020**, 11, 2495.
- (51) Moučka, F.; Nezbeda, I. Detection and Characterization of Structural Changes in the Hard-Disk Fluid under Freezing and Melting Conditions. *Phys. Rev. Lett.* **2005**, 94, 040601.
- (52) Reis, P. M.; Ingale, R. A.; Shattuck, M. D. Crystallization of a Quasi-Two-Dimensional Granular Fluid *Phys. Rev. Lett.* **2006**, 96, 258001.
- (53) Ebert, F.; Maret, G.; Keim, P. Partial clustering prevents global crystallization in a binary 2D colloidal glass former *Eur. Phys. J. E* **2009**, 29, 311-318
- (54) Lotito, V.; Zambelli, T. Pattern Formation in Binary Colloidal Assemblies: Hidden Symmetries in a Kaleidoscope of Structures *Langmuir* **2018**, 34, 7827-7843.
- (55) Lotito, V.; Zambelli, T. A Journey Through the Landscapes of Small Particles in Binary Colloidal Assemblies: Unveiling Structural Transitions from Isolated Particles to Clusters upon Variation in Composition. *Nanomaterials* **2019**, 9, 921.
- (56) Lotito, V.; Zambelli, T. Pattern detection in colloidal assembly: A mosaic of analysis techniques *Adv. Colloid Interface Sci.* **2020**, 2844, 102252.

Table of Contents Graphic

